Facile One-step Redox Synthesis of Bi2o2co3/bi2o3/bi Ternary Photocatalyst Without Additional Carbon Source

Qiao Chen
Qingdao Agricultural University
Xuefang Lan
Qingdao Agricultural University
Guihua Zhu
Qingdao Animal Husbandry and Veterinary Research Institute
Lili Wang
Qingdao Agricultural University
Jinsheng Shi (jsshiqn123@126.com)
Qingdao Agricultural University https://orcid.org/0000-0003-2219-5956

Research Article

Keywords: one-step redox method, ternary catalyst, non-additional carbon source, photocatalytic water purification

Posted Date: March 15th, 2021

DOI: https://doi.org/10.21203/rs.3.rs-174092/v1

Abstract

Construction of heterojunction and decoration of cocatalyst are two vital strategies to accelerate migration of charge carriers. However, the fabrication routs of multi-composites are usually complex and expensive. In this work, $Bi_2O_2CO_3$/Bi_2O_3/Bi ternary composite was fabricated via a facile one-step redox reaction. Ethylene glycol was selected as the solvent during the whole reaction process. Moreover, ethylene glycol as an excellent reductant can reduce Bi^{3+} into metallic Bi^0 and itself is oxidized to CO_3^{2-}, which would react with Bi_2O_3 to generate $Bi_2O_2CO_3$ without additional carbon source. Component proportions in ternary composites were optimized by the control of the ratios of raw materials. Under simulate solar light, Bi-based ternary composites exhibited enhanced photodegradation efficiencies for multifarious pollutants in comparison with single and binary samples. The enhanced photocatalytic activities were ascribed to accelerated migration rate of charge carriers owing to the construction of heterojunction and decoration of cocatalyst.

1. Introduction

Water contamination has become a highly concerned issue owing to its close relationship with drinking water quality and human health [1–4]. It is estimated that millions of serious illness and even death are caused by water pollution every year [5]. Therefore, developing rapid, efficient and economical technologies has become a global concern [6, 7]. As we know, semiconductor-based photocatalysis, as one of the most promising strategies, has aroused widespread attention in removal of hazardous organic pollutants [8, 9]. Efficient photogenerated charge carriers separation and migration is one of the main factors to improve photocatalytic activity [10–14]. Up to now, construction of heterojunction is considered as one of the effective strategies to inhibit charge recombination and enhance photocatalytic efficiency because of staggered band alignments between two semiconductor components [15–18]. In general, photogenerated electrons (holes) on the higher conduction (lower valence) band of semiconductor would migrate to another one with a lower conduction (higher valence) band, which could realize spatial separation of charge carriers and suppress their recombination [19]. Except heterojunction, modification of co-catalysts such as noble metals onto surface of materials is also a crucial method to accelerate separation of electron-hole pairs [20–22]. When the position of Fermi level of metals below the conduction band (CB) of catalysts, photogenerated electrons on the CB of catalysts can rapidly transfer to the surfaces of metals. Noble metals could act as a reservoir of electrons, preventing the recombination of charge carriers and strengthening the quantum efficiency of photocatalytic activity [23, 24]. Besides, the Schottky barrier at heterojunction-metal interface can further retard electron-hole recombination owing to the internal electric field [25]. However, the scale application of noble metals is suppressed because of their high price. Some semi-metal such as metallic bismuth (Bi), as an abundant earth element with high carrier mobility and low effective electron mass, could also act as an effective co-catalyst and extensively be used in photocatalysis [26, 27].

Recently, Bi-based composites have been well explored for efficient photocatalysts [28, 29]. As we know, current their synthesis usually need two or multi steps, which are expensive and laborious. Herein, $Bi_2O_2CO_3/Bi_2O_3/Bi$ ternary composite was synthesized through a facile one-step redox reaction process, which is time-saving, labor-saving and low-cost. During synthesis, ethylene glycol (EG) is selected as solvent for the whole reaction process, which also as an excellent reducing agent can reduce Bi^{3+} into metallic Bi^0 and itself is oxidized to CO_3^{2-}, reacting with Bi_2O_3 to generate $Bi_2O_2CO_3$ without any additional carbon source. The ternary composites with different component proportions are obtained by the control of the ratios of raw materials. Compared with single or binary catalysts, $Bi_2O_2CO_3/Bi_2O_3/Bi$ composites exhibit increased photodegradation activities toward multifarious organic pollutants under solar light irradiation.

2. Results And Discussion

2.1 Crystal structure and formation mechanism of BOC samples

$Bi_2O_2CO_3/Bi_2O_3/Bi$ ternary composites were fabricated via a facile one-pot solvothermal route (Fig. 1a). Figure 2a presents the X-Ray diffraction (XRD) patterns of samples. When the molar ratio of Bi^{3+}: OH^- is 2.7, only $Bi_2O_2CO_3$ peaks are observed for BOC-1 composite. As OH^- dosages is increased, both diffraction peaks of $Bi_2O_2CO_3$, Bi_2O_3 and metallic Bi could be clearly seen for BOC-2, BOC-3, BOC-4 and BOC-5, which are ascribed to orthorhombic $Bi_2O_2CO_3$ (JCPDS 84-1752) [30], cubic Bi_2O_3 (JCPDS 74-1375) [31] and Bi (JCPDS 85-1329) [32], respectively. However, diffraction peaks of Bi_2O_3 would disappear and only signals of $Bi_2O_2CO_3$ and Bi are observed with the increase of molar ratio of Bi^{3+}: OH^- to 4.7 (BOC-6). As for BOC composites, the colors of samples accompany with the increase of OH^- dosages, which change from white to gray, then to dark grey (Fig. 2b). The color variations may be related with the content of metallic Bi because diffraction peaks of metallic Bi gradually increases with the increase of OH^- dosages. A possible generation mechanism of Bi-based ternary composite is discussed. In this reaction system, EG is easily oxidized to glyoxal then to oxalic acid. Oxalic acid is unstable and easily decomposed into CO_3^{2-} via the cleavage of C-C bond, which could be used to prepare $Bi_2O_2CO_3$ (Fig. 2c). Bi_2O_3 is produced through ion exchange route, which utilizes $Bi(NO)_3$ as Bi source and NaOH as OH^- source. Once combining Bi^{3+} and OH^- together, $Bi(OH)_3$ precipitate is obtained then transforms to Bi_2O_3 after hydrothermal treatment owing to its instability (Fig. 2d). $Bi_2O_2CO_3$ is generated by the simple combination of Bi_2O_3 with CO_3^{2-} (Fig. 2e). In addition, EG as an excellent reductant can reduce Bi^{3+} to metallic Bi (Fig. 2f).

2.2 XPS analysis

X-ray photoelectron spectroscopy (XPS) is utilized to study the compositions of composites [33]. In Fig. 3a, full survey spectrum confirms the existence of Bi, O and C elements in BOC-3. As can be seen in Fig. 3b, four peaks of Bi 4f energy level are noticed, in which two Bi signals at 164.2 and 158.9 eV are belonged to Bi $4f_{5/2}$ and Bi $4f_{7/2}$, respectively, ascribing to Bi^{3+} in $Bi_2O_2CO_3$ and Bi_2O_3 [34, 35]. The other two signals locate at 162.0 and 156.8 eV, which are corresponded to metallic Bi^0 [36]. The asymmetric profile of O1s signal suggests that more than one kind of oxygen species exist. In Fig. 3c, the O1s spectrum can be split into three peaks at binding energies of 531.0, 530.2 and 529.8 eV. The peak at 531.0 eV is ascribed to the surface hydroxyl groups adsorbed on material [37]. Besides, the signals at 530.2 and 529.8 eV are attributed to the characteristics of C-O bond in $[CO_3]^{2-}$ layers and Bi-O bond in $[Bi_2O_2]^{2+}$ layers [38, 39]. As shown in Fig. 3d, C 1 s signal of BOC-3 can be split into three peaks at 288.3, 285.9 and 284.6 eV, which are assigned to CO_3^{2-} in $Bi_2O_2CO_3$, O-bearing bonding (C-OH), and sp^2 carbon, respectively [40].

2.3 Morphology and microstructure analysis

Morphology and microstructure of composite are studied by scanning electron microscope (SEM) and transmission electron microscope (TEM). As shown in Fig. 4a, BOC-3 sample is composed of irregular micro-plates with size of about 1–2 μm. The thickness of plates is approximately 50 nm. High resolution transmission electron microscope (HR-TEM) image of BOC-3 confirms the detailed structure. In Fig. 4b, it is clearly that three different lattice fringes with d-spacing of 0.29, 0.33 and 0.26 nm, which are attributed to (1 6 1) plane of $Bi_2O_2CO_3$, (0 1 2) plane of metallic Bi and (1 2 3) plane of B_2O_3, respectively. SEM image and corresponding element distributions of BOC-3 are shown in Fig. 4c-f, which indicate Bi, O and C elements are evenly distributed throughout the micro-plate. These results suggest that Bi-based composites are successfully fabricated.

2.4 Photocatalytic activity of samples

Photodegradation ability of sample is studied under solar light irradiation by choosing TEC and BPA as model organic pollutants. In Fig. 5a, BOC-1 presents relatively low photodegradation efficiency owing to the large band gap of $Bi_2O_2CO_3$, while photocatalytic activities of BOC-5 and BOC-6 obviously enhance because of the construction of heterojunction and modification of metallic Bi. Furthermore, after decoration of Bi_2O_3 and metallic Bi onto $Bi_2O_2CO_3$, degradation efficiencies of samples further improve. BOC-3 presents the highest degradation efficiency and 97.8% of TEC is removed within 150 min, which is attributed to the synergy effect of heterojunction and co-catalyst. Figure 5c exhibits the kinetic constants of BOC for TEC degradation. BOC-2, BOC-3 and BOC-4 present enhanced degradation rates, which is determined to be 0.016, 0.024 and 0.014 min^{-1}, much higher than that of other samples. In addition, BPA is also used as target pollutant to investigate photocatalytic activity of samples. Figure 5b shows the degradation curves of BOC toward BPA under simulated solar irradiation and relevant kinetic constants are calculated in Fig. 5d. Similarly, BPA degradation rates of BOC-2, BOC-3 and BOC-4 obviously enhance in comparison with other samples. In order to further confirm the efficient photocatalytic performance of

ternary composites, the degradations of various pollutants including methyl orange (MO), methylene blue (MB) and rhodamine B (RhB) are also studied. As shown in Fig. 5e, ternary samples exhibit enhanced photodegradation efficiencies. Cycling experiments of BOC-3 for TEC and BPA degradation are carried out to determine its stability. As can be seen from Fig. 5f, TEC and BPA photodegradation efficiencies of BOC-3 change little after five cycles, implying its high stability.

2.5 Photocatalytic mechanism

Photoluminescence (PL) test is an effective technology to investigate the separation and migration of photogenerated electrons-holes pairs in materials due to PL emission mainly originates from the recombination of electrons and holes [41]. Figure 6a presents PL spectra of as-synthesized materials in the range of 320–700 nm under the excitation of 285 nm. The order of emission peaks intensity is BOC-3 < BOC-2 < BOC-4 < BOC-5 < BOC-6 < BOC-1, which is consistent with the photodegradation efficiency of pollutants. The weak peak intensity indicates the effective separation and transfer of photoinduced charge carriers. The interfacial charge separation and transfer dynamics of material during photocatalytic process are also studied by electrochemical impedance spectroscopy (EIS) [42]. As shown in Fig. 6b, these curves are fitted with the equivalent circuit of $R_s(QR_f)(QR_{ct})$, where R_s, Q, R_f and R_{ct} are electrolyte resistance, constant phase element, layer resistance of materials and charge transfer resistance, respectively. Similarly, the order of semicircle arc is BOC-3 < BOC-2 < BOC-4 < BOC-5 < BOC-6 < BOC-1, which is consistent with PL analysis and photodegradation efficiency of pollutants. Typically, a smaller semicircle means smaller resistance value, which expresses faster interfacial charges migration rates. These results suggest that the construction of heterojunction and decoration of cocatalyst lead to the efficient separation of photogenerated charge carriers, further enhancing photocatalytic activity.

3. Conclusion

In summary, $Bi_2O_2CO_3/Bi_2O_3$/Bi ternary composite was fabricated via a facile one-step redox reaction without additional carbon source. During synthesis, EG is selected as solvent in the whole fabrication process. Besides, EG is also an effective reducing agent, which can reduce Bi^{3+} into metallic Bi and itself is oxidized to CO_3^{2-}, reacting with Bi_2O_3 to construct $Bi_2O_2CO_3$. In comparison with single or binary samples, Bi-based composites exhibit largely increased photodegradation abilities for multifarious pollutants such as BPA, TEC, MO, ME and RhB under solar light irradiation. The enhanced photocatalytic activities are ascribed to accelerated migration rate of charge carriers owing the synergy effect of heterojunction and co-catalyst.

Declarations

Acknowledgements

This work was supported by National Natural Science Foundation of China (No. 11804180), Youth Foundation of Qingdao Application and Basic Research (No. 19-6-2-16-cg) and Doctoral Fund of Qingdao Agricultural University (No. 663/1118005).

References

1. L. Wang, A. Kaeppler, D. Fischer, J. Simmchen, Photocatalytic TiO_2 micromotors for removal of microplastics and suspended matter. ACS Appl Mater Interfaces **11**, 32937–32944 (2019)
2. F.J. Beltrán, M. Checa, Comparison of graphene oxide titania catalysts for their use in photocatalytic ozonation of water contaminants: Application to oxalic acid removal. Chem. Eng. J. **385**, 123922 (2020)
3. N. Negishi, M. Sugasawa, Y. Miyazaki, Y. Hirami, S. Koura, Effect of dissolved silica on photocatalytic water purification with a TiO_2 ceramic catalyst. Water Res **150**, 40–46 (2019)
4. X. Zhang, S. Liu, A. Salim, S. Seeger, Hierarchical structured multifunctional self-cleaning material with durable superhydrophobicity and photocatalytic functionalities. Small **15**, 1901822 (2019)
5. R. Qadri, M.A. Faiq, Freshwater pollution: Effects on aquatic life and human health, in *Fresh water pollution dynamics and remediation*, ed. by H. Qadri, R.A. Bhat, M.A. Mehmood, G.H. Dar (Springer Singapore, Singapore, 2020), pp. 15–26
6. S. Bolisetty, M. Peydayesh, R. Mezzenga, Sustainable technologies for water purification from heavy metals: review and analysis. Chem. Soc. Rev. **48**, 463–487 (2019)
7. S.T. Khan, A. Malik, Engineered nanomaterials for water decontamination and purification: From lab to products. J. Hazard. Mater. **363**, 295–308 (2019)
8. G. Zhang, X. Zhang, Y. Meng, G. Pan, Z. Ni, S. Xia, Layered double hydroxides-based photocatalysts and visible-light driven photodegradation of organic pollutants: A review. Chem. Eng. J. **392**, 123684 (2020)
9. D. Yu, L. Li, M. Wu, J.C. Crittenden, Enhanced photocatalytic ozonation of organic pollutants using an iron-based metal-organic framework. Appl Catal B, Environ **251**, 66–75 (2019)
10. Q. Zhao, A. Hazarika, X. Chen, S.P. Harvey, B.W. Larson, G.R. Teeter et al., High efficiency perovskite quantum dot solar cells with charge separating heterostructure. Nat Commun **10**, 2842 (2019)
11. X. Ning, B. Lu, Z. Zhang, P. Du, H. Ren, D. Shan et al., An efficient strategy for boosting photogenerated charge separation by using porphyrins as interfacial charge mediators. Angew. Chem. Int. Edit. **58**, 16800–16805 (2019)
12. S. Tu, Y. Zhang, A.H. Reshak, S. Auluck, L. Ye, X. Han et al., Ferroelectric polarization promoted bulk charge separation for highly efficient CO_2 photoreduction of SrBi4Ti4O15. Nano Energy **56**, 840–850 (2019)
13. Q. Shi, M. Zhang, Z. Zhang, Y. Li, Y. Qu, Z. Liu et al., Energy and separation optimization of photogenerated charge in $BiVO_4$ quantum dots by piezo-potential for efficient gaseous pollutant degradation. Nano Energy **69**, 104448 (2020)

14. Z. Jiang, W. Miao, X. Zhu, G. Yang, Z. Yuan, J. Chen et al., Modifying lewis base on TiO2 nanosheets for enhancing CO_2 adsorption and the separation of photogenerated charge carriers. Appl Catal B, Environ **256**, 117881 (2019)
15. Q. Wang, M. Nakabayashi, T. Hisatomi, S. Sun, S. Akiyama, Z. Wang et al., Oxysulfide photocatalyst for visible-light-driven overall water splitting. Nat. Mater. **18**, 827–832 (2019)
16. Z. Hu, X. Zhang, Q. Yin, X. Liu, X. Jiang, Z. Chen et al., Highly efficient photocatalytic hydrogen evolution from water-soluble conjugated polyelectrolytes. Nano Energy **60**, 775–783 (2019)
17. J.S. Schubert, J. Popovic, G.M. Haselmann, S.P. Nandan, J. Wang, A. Giesriegl et al., Immobilization of Co, Mn, Ni and Fe oxide co-catalysts on TiO_2 for photocatalytic water splitting reactions. J Mater Chem A **7**, 18568–18579 (2019)
18. D. Zeng, T. Zhou, W.-J. Ong, M. Wu, X. Duan, W. Xu et al., Sub-5 nm ultra-fine FeP nanodots as efficient co-catalysts modified porous g-C_3N_4 for precious-metal-free photocatalytic hydrogen evolution under visible light. ACS Appl Mater Interfaces **11**, 5651–5660 (2019)
19. C. Sotelo-Vazquez, R. Quesada-Cabrera, M. Ling, D.O. Scanlon, A. Kafizas, P.K. Thakur et al., Evidence and effect of photogenerated charge transfer for enhanced photocatalysis in WO_3/TiO_2 heterojunction films: A computational and experimental study. Adv. Funct. Mater. **27**, 1605413 (2017)
20. L. Meng, Z. Chen, Z. Ma, S. He, Y. Hou, H.-H. Li et al., Gold plasmon-induced photocatalytic dehydrogenative coupling of methane to ethane on polar oxide surfaces. Energy Environ Sci **11**, 294–298 (2018)
21. A. Zada, P. Muhammad, W. Ahmad, Z. Hussain, S. Ali, M. Khan et al., Surface plasmonic-assisted photocatalysis and optoelectronic devices with noble metal nanocrystals: Design, synthesis, and applications. Adv. Funct. Mater. **30**, 1906744 (2020)
22. B. Ma, X. Li, D. Li, K. Lin, A difunctional photocatalytic H_2 evolution composite co-catalyst tailored by integration with earth-abundant material and ultralow amount of noble metal. Appl Catal B, Environ **256**, 117865 (2019)
23. X. Liu, J. Iocozzia, Y. Wang, X. Cui, Y. Chen, S. Zhao et al., Noble metal–metal oxide nanohybrids with tailored nanostructures for efficient solar energy conversion, photocatalysis and environmental remediation. Energy Environ Sci **10**, 402–434 (2017)
24. D. Ma, J.-W. Shi, D. Sun, Y. Zou, L. Cheng, C. He et al., Au decorated hollow ZnO@ZnS heterostructure for enhanced photocatalytic hydrogen evolution: The insight into the roles of hollow channel and Au nanoparticles. Appl Catal B, Environ **244**, 748–757 (2019)
25. J. Jiao, Y. Wei, Y. Zhao, Z. Zhao, A. Duan, J. Liu et al., AuPd/3DOM-TiO_2 catalysts for photocatalytic reduction of CO_2: High efficient separation of photogenerated charge carriers. Appl Catal B, Environ **209**, 228–239 (2017)
26. Q. Hao, R. Wang, H. Lu, W. Xie Ca, Ao, D. Chen et al., One-pot synthesis of C/Bi/Bi_2O_3 composite with enhanced photocatalytic activity. Appl Catal B, Environ **219**, 63–72 (2017)

27. L. Xu, W. Chen, S. Ke, S. Zhang, M. Zhu, Y. Zhang et al., Construction of heterojunction $Bi/Bi_5O_7I/Sn_3O_4$ for efficient noble-metal-free Z-scheme photocatalytic H2 evolution. Chem. Eng. J. **382**, 122810 (2020)
28. X. Li, W. Zhang, J. Li, G. Jiang, Y. Zhou, S. Lee et al., Transformation pathway and toxic intermediates inhibition of photocatalytic NO removal on designed Bi metal@defective $Bi_2O_2SiO_3$. Appl Catal B, Environ **241**, 187–195 (2019)
29. K. Wang, Y. Li, G. Zhang, J. Li, X. Wu, 0D Bi nanodots/2D Bi_3NbO_7 nanosheets heterojunctions for efficient visible light photocatalytic degradation of antibiotics: Enhanced molecular oxygen activation and mechanism insight. Appl Catal B, Environ **240**, 39–49 (2019)
30. J. Ding, Z. Dai, F. Qin, H. Zhao, S. Zhao, R. Chen, Z-scheme $BiO_{1-x}Br/Bi_2O_2CO_3$ photocatalyst with rich oxygen vacancy as electron mediator for highly efficient degradation of antibiotics. Appl Catal B, Environ **205**, 281–291 (2017)
31. L. Hu, G. Zhang, Q. Wang, Y. Sun, M. Liu, P. Wang, Facile synthesis of novel Co_3O_4-Bi_2O_3 catalysts and their catalytic activity on bisphenol A by peroxymonosulfate activation. Chem. Eng. J. **326**, 1095–1104 (2017)
32. G. Zhang, W. Wang, X. Li, Enhanced thermoelectric properties of core/shell heterostructure nanowire composites. Adv Mater **20**, 3654–3656 (2008)
33. W.H.M. Abdelraheem, M.K. Patil, M.N. Nadagouda, D.D. Dionysiou, Hydrothermal synthesis of photoactive nitrogen- and boron- codoped TiO_2 nanoparticles for the treatment of bisphenol A in wastewater: Synthesis, photocatalytic activity, degradation byproducts and reaction pathways. Appl Catal B, Environ **241**, 598–611 (2019)
34. Y. Zhang, L. Wang, F. Dong, Q. Chen, H. Jiang, M. Xu et al., Non-additional carbon source one-step synthesis of $Bi_2O_2CO_3$-based ternary composite for efficient Z-scheme photocatalysis. J. Colloid Interface Sci. **536**, 575–585 (2019)
35. L. Shan, Y. Liu, C. Ma, L. Dong, L. Liu, Z. Wu, Enhanced photocatalytic performance in Ag+-induced $BiVO_4$/β-Bi_2O_3 heterojunctions. Eur. J. Inorg. Chem. **2016**, 232–239 (2016)
36. Y. Ma, Y. Zhang, L. Wang, C. Wang, X. Diao, J. Shi, Single solvent-induced one-step solvothermal method: A general strategy for controllable synthesis of ternary and multiplex Bi-based composites. J. Alloys Compd. **784**, 405–413 (2019)
37. L. Cai, Z. Lin, M. Wang, F. Pan, J. Chen, Y. Wang et al., Improved interfacial H_2O supply by surface hydroxyl groups for enhanced alkaline hydrogen evolution. J Mater Chem A **5**, 24091–24097 (2017)
38. L. Zhao, Y. Chen, Y. Feng, D. Wu, Oxidation of acetaminophen by Green rust coupled with Cu(II) via dioxygen activation: The role of various interlayer anions (CO_3^{2-}, SO_4^{2-}, Cl^-). Chem. Eng. J. **350**, 930–938 (2018)
39. Y. Bian, Y. Ma, Y. Shang, P. Tan, J. Pan, Self-integrated β-Bi_2O_3/$Bi_2O_{2.33}$@$Bi_2O_2CO_3$ ternary composites: Formation mechanism and visible light photocatalytic activity. Appl Surf Sci **430**, 613–624 (2018)

40. J. Hu, D. Chen, N. Li, Q. Xu, H. Li, J. He et al., Recyclable carbon nanofibers@hierarchical I-doped $Bi_2O_2CO_3$–MoS_2 membranes for highly efficient water remediation under visible-light irradiation. ACS Sustain Chem Eng **6**, 2676–2683 (2018)
41. W. Lei, Y. Mi, R. Feng, P. Liu, S. Hu, J. Yu et al., Hybrid 0D–2D black phosphorus quantum dots–graphitic carbon nitride nanosheets for efficient hydrogen evolution. Nano Energy **50**, 552–561 (2018)
42. W. Zhao, Y. Feng, H. Huang, P. Zhou, J. Li, L. Zhang et al., A novel Z-scheme Ag_3VO_4/$BiVO_4$ heterojunction photocatalyst: Study on the excellent photocatalytic performance and photocatalytic mechanism. Appl Catal B, Environ **245**, 448–458 (2019)

Figures

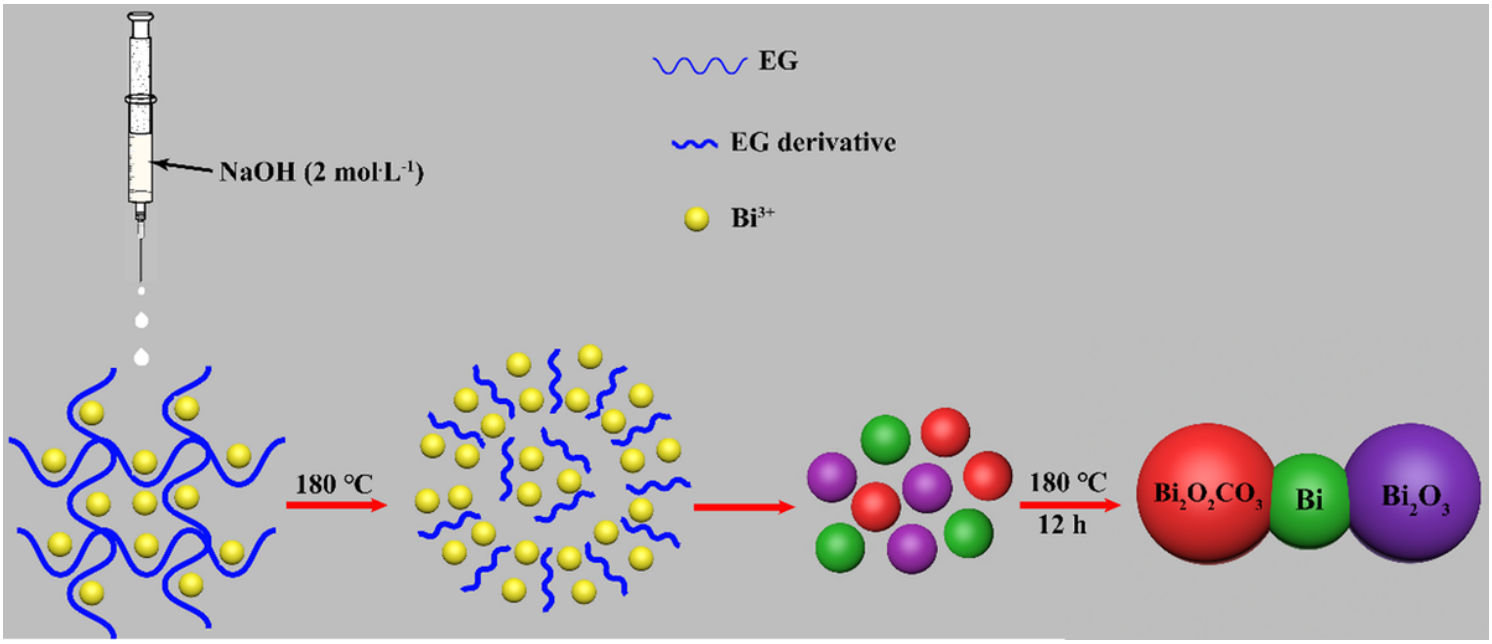

Figure 1

Overall flowchart for the fabrication of Bi2O2CO3/Bi2O3/Bi.

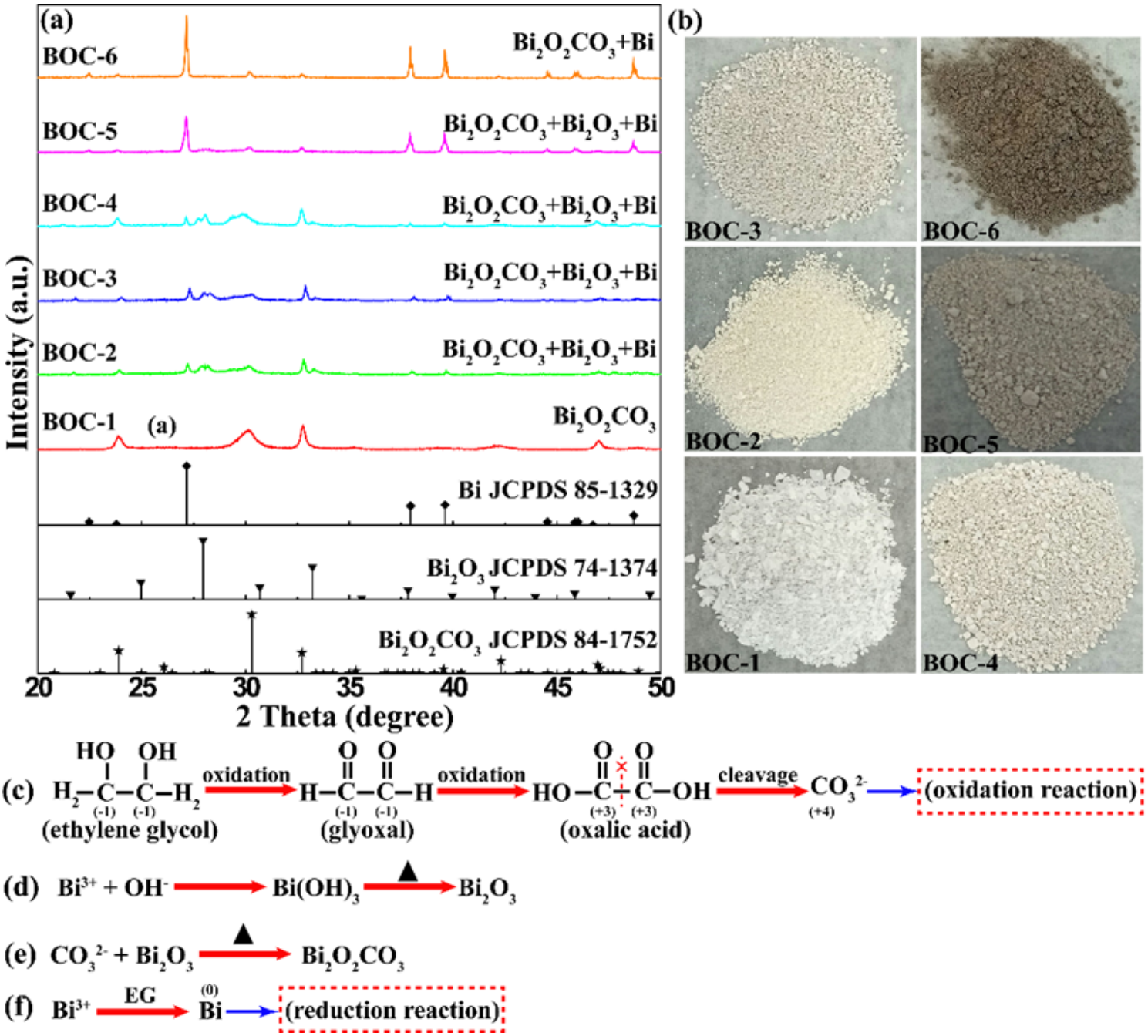

Figure 2

(a) XRD patterns and (b) photographs of the synthesized samples. (c)-(f) Formation mechanism of Bi-based ternary composites.

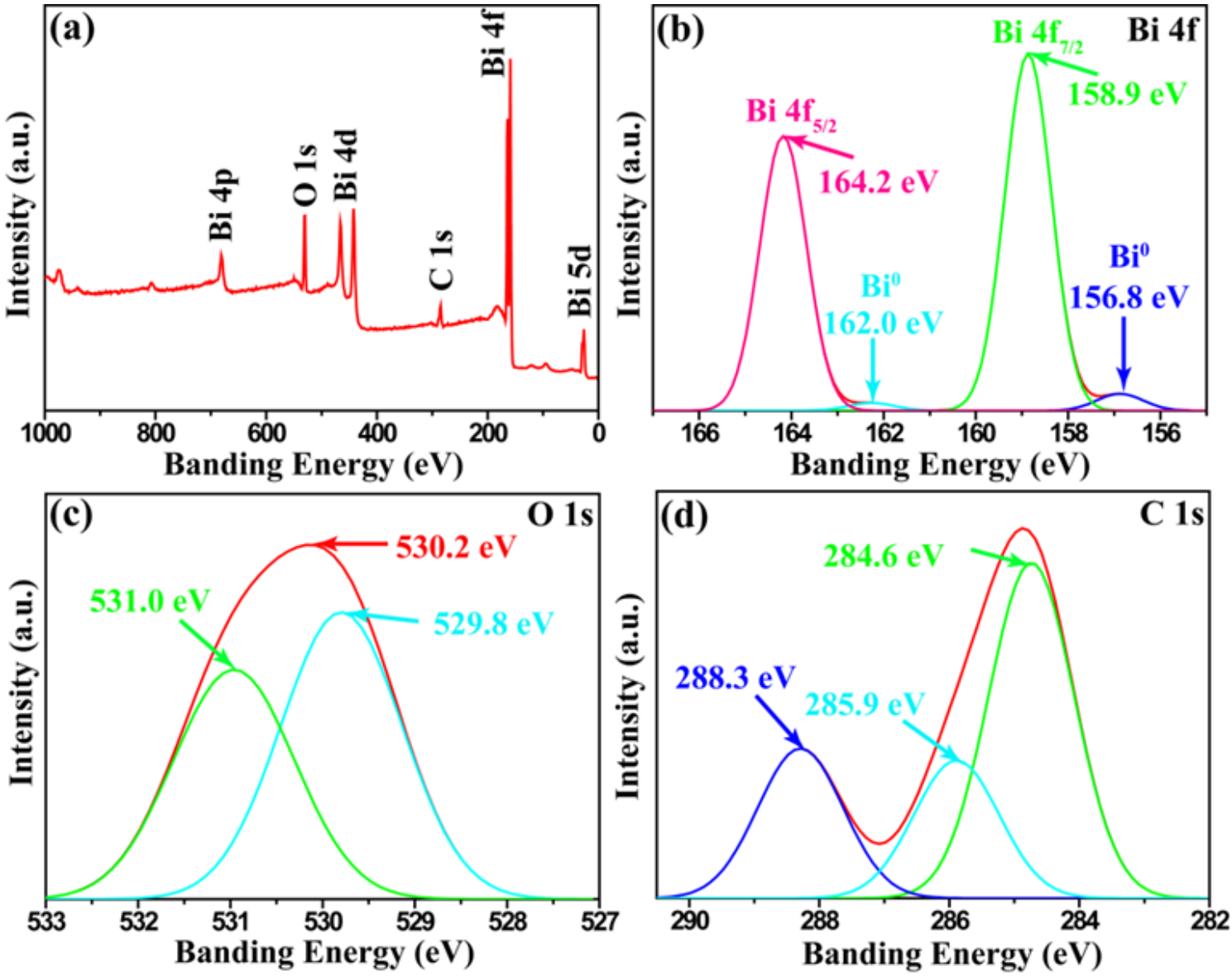

Figure 3

XPS spectra of BOC-3 sample (a) survey spectrum, (b) high resolution XPS spectra of Bi 4f, (c) O 1s and (d) C 1s.

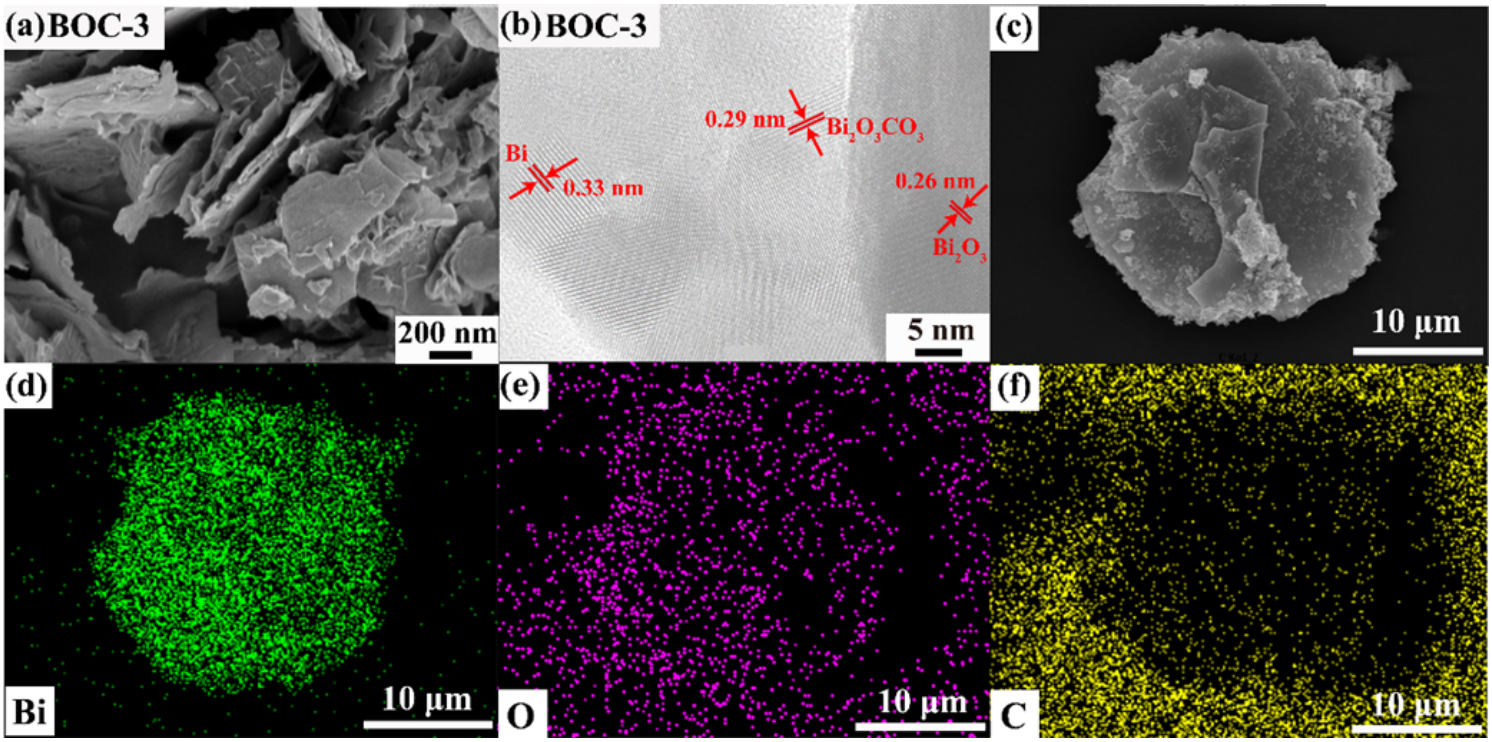

Figure 4

(a) SEM image and (b) HR-TEM image of BOC-3 composite. (c) SEM image and corresponding elemental mappings of (d) Bi, (e) O and (f) C of BOC-3.

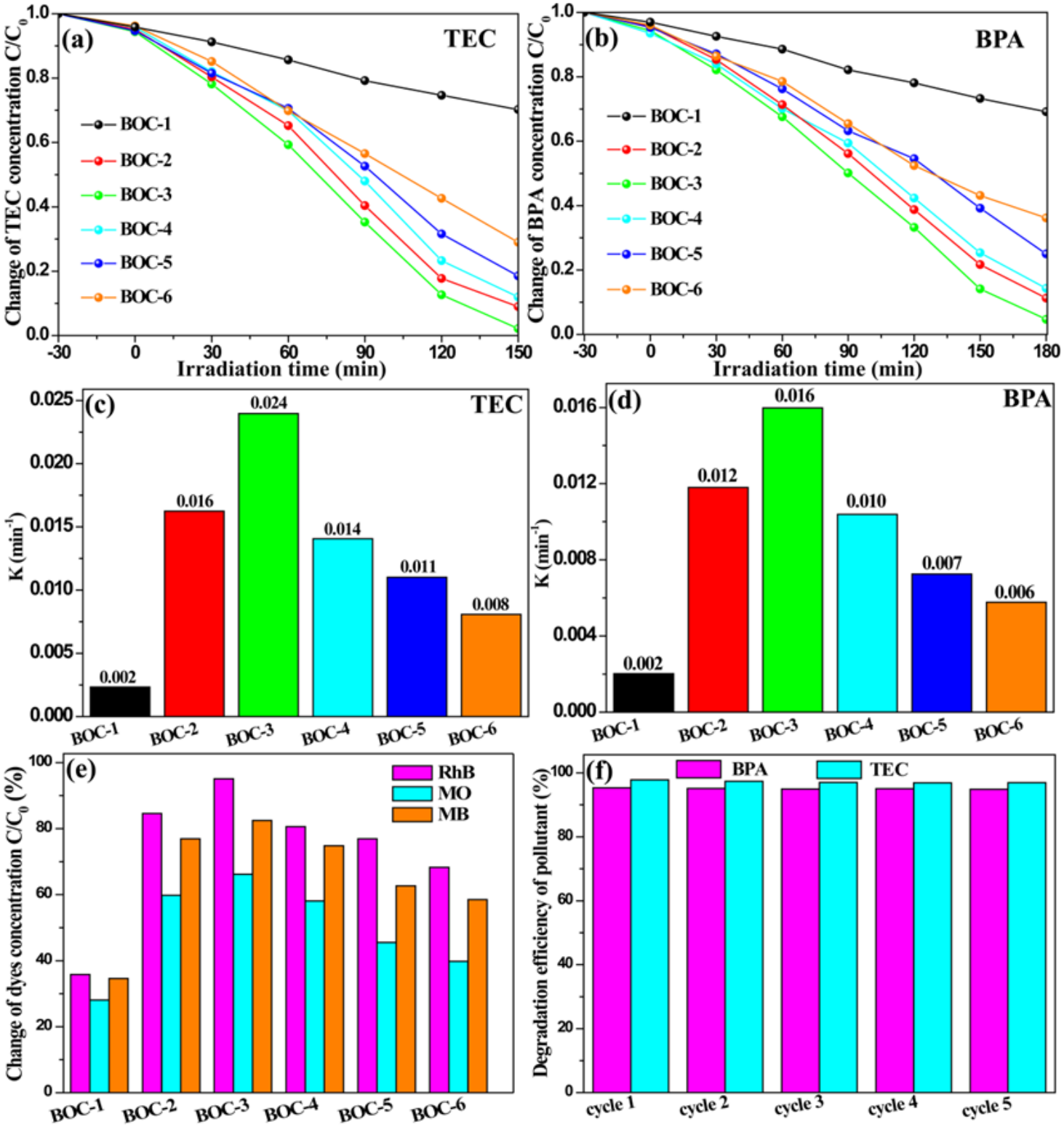

Figure 5

(a) TEC and (b) BPA photodegradations of different samples under solar light irradiation. Apparent rate constants of different samples for (c) TEC and (d) BPA photodegradations. (e) Apparent rate constants of as-prepared samples for photodegradations of other pollutants (RhB, MO, MB). (f) Cycling tests of BOC-3 for the degradations of BPA and TEC under solar light illumination.

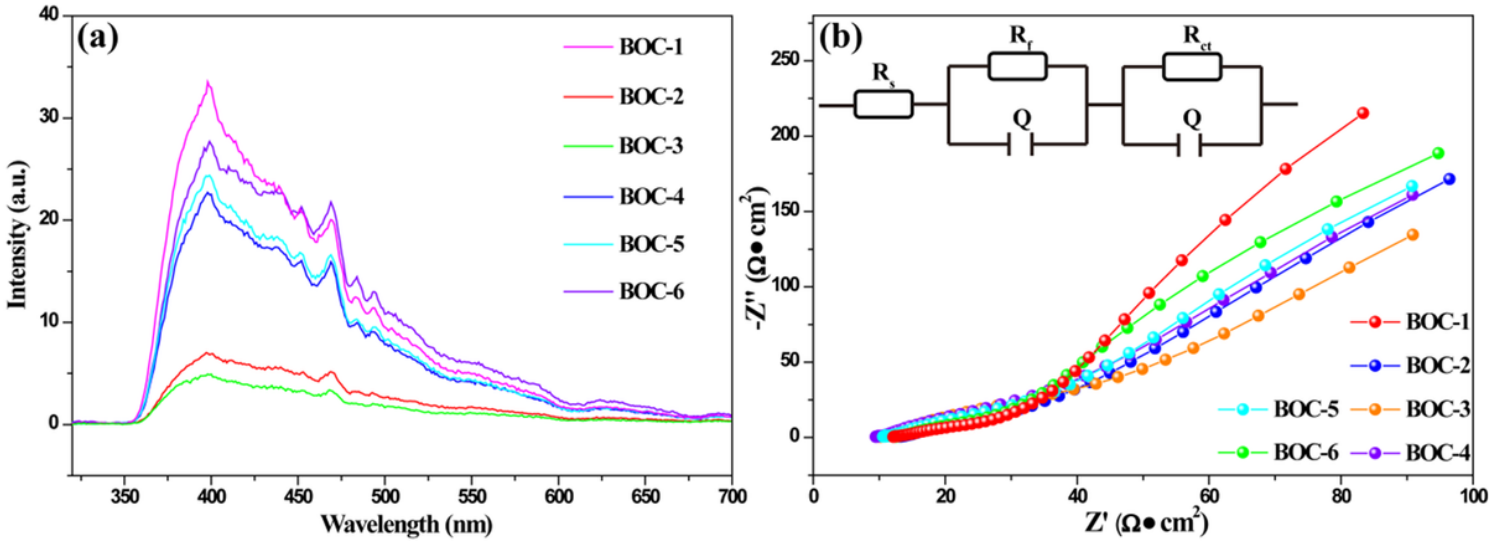

Figure 6

(a) Comparison of the PL spectra of a series of samples at excitation wavelength of 285 nm. (b) EIS plots of the samples under solar light irradiation and corresponding schematic (inset) of the equivalent circuit obtained by fitting the EIS results.